PROCEEDINGS, Thirty-Eighth Workshop on Geothermal Reservoir Engineering
Stanford University, Stanford, California, February 11-13, 2013
SGP-TR-198

EXPERIMENTAL INVESTIGATION OF BRINE-CO_2 FLOW THROUGH A NATURAL FRACTURE: PERMEABILITY INCREASES WITH CONCURRENT DISSOLUTION/REPRECIPITATION REACTIONS

Megan M. Smith, Stuart D.C. Walsh, Walt W. McNab, and Susan A. Carroll

Atmospheric Earth and Energy Division
Lawrence Livermore National Laboratory
7000 East Avenue, L-231
Livermore, CA, 94550, U.S.A.
megan@llnl.gov

ABSTRACT

CO_2 has been proposed as an attractive alternative heat-transmission fluid for engineered geothermal systems, but the geochemical and geomechanical impacts of elevated CO_2 content on reservoir sustainability are currently not well understood. The potential effects of using CO_2 as a heat-exchange fluid on fracture flow and permeability were investigated by means of a 60-day core-flood experiment in which a pre-existing fracture was exposed to CO_2-acidified brine at 200 °C and 25 MPa. Differential pressures decreased continuously, indicating increasing fracture permeability during both CO_2-free and high pCO_2 fluid flow, and changes in solution chemistry show enhanced mineral dissolution with the introduction of CO_2. Fracture aperture and geometry were analyzed by high-resolution X-ray tomography before and after the core-flooding reaction. Changes in solution chemistry were used to identify the likely reactions responsible for dissolution features and porosity increases noted along some fracture regions, as well as the solid precipitates observed in wide-aperture zones. Particle Image Velocimetry analysis was applied to the tomography data to measure local deformation. Experimental and preliminary simulation results are presented with discussion of implications for CO_2-EGS.

INTRODUCTION

Supercritical CO_2 has been proposed as an alternative heat transmission fluid for Engineered Geothermal Systems (EGS) (Brown, 2000). The benefits due to its lower viscosity and greater buoyancy compared to water are expected to outweigh any reduction in performance arising from its lower heat capacity, resulting in enhanced heat extraction (Pruess, 2006). In addition, expected losses of heat transmitting fluids during reservoir circulation could, in the case of CO_2, result in additional carbon storage (provided that no leakage pathways to the surface exist).

Although the physical properties of CO_2 may make it an advantageous alternative heat transmission fluid, less is known regarding the chemical effects of substituting CO_2 for water in high-temperature reservoir systems. Currently, the dissolution and precipitation behavior of many minerals is not well understood at temperatures typical of geothermal systems, and less information exists to constrain the geochemical effects of rock-CO_2-water interactions. Recent experimental work (e.g., Ueda et al., 2005; Suto et al., 2007; McGrail et al., 2009; Smith et al., 2013) demonstrates that "wet" CO_2 and CO_2-saturated water can react readily with many constituent minerals at elevated temperatures and/or high pCO_2 levels.

Whether increased reactivity in fractured systems will prove beneficial to sustained system permeability (by increasing fracture aperature), or detrimental (through weakening of fracture walls and aperture closure) is not clear at this time. Permeability decreases with ongoing mineral dissolution have been noted in fractured granite (Morrow et al., 2001), novaculite (Polak et al., 2003), and quartz monzonite (Carlson et al., 2005) at elevated temperature under CO_2-free flow conditions. At lower temperatures in fractured carbonates, however, permeability increases were noted as a result of the introduction of chemically perturbed fluids (Polak et al., 2004; Ellis et al., 2011). Additionally, the precipitation of carbonate minerals (resulting from high levels of dissolved metals and available $CO_{2(aq)}$ in a CO_2-EGS reservoir) may counter any permeability increases if the precipitates accumulate along fracture walls.

Previous modeling work by Wolery and Carroll (2010) focused on the Ohaaki-Broadlands geothermal site in the Taupo Volcanic Zone, New Zealand, as a natural analog site for a potential CO_2-EGS site. The hottest fluids at this site carry high levels of CO_2 from fractures in the deep greywacke basement rock into the overlying reservoir formations. Geochemical calculations over temperatures of 100-300 °C, up to 1.2 mol/L dissolved CO_2, and using a range of likely mineral assemblages concluded that many reported alteration minerals within the greywacke do not appear to be thermodynamically stable as a group, and that kinetic controls likely play a role in the resulting assemblage. Along with calcite, various sheet silicate minerals (chiefly varieties of muscovite and chlorite) were shown to react strongly with high pCO_2 fluids, and in some cases re-precipitate. Uncertainty in existing equilibrium data and a lack of high-temperature kinetic expressions for several of these sheet silicates prompted us to further explore the reactivity of one particular sheet silicate observed in the greywacke formation (Mg-rich chlorite; Smith et al., 2013). The objective of this work was to react a fractured greywacke sample with CO_2-enriched fluids to obtain direct information regarding the reactivity of certain minerals under these conditions and observe the response of the fracture under disequilibrium conditions.

EXPERIMENTAL & MODEL METHODS

A 63-day experiment was conducted to monitor the geochemical and permeability response of a fractured greywacke rock core to 200 °C, 5.5 MPa pCO_2 fluid. Details of sample characterization, treatment, and data analysis are given below.

Sample Characterization and Preparation

Bulk rock samples of greywacke rock units stratigraphically consistent with the basement greywacke identified in geothermal wellbores were obtained from surface outcropping near the Ohaaki-Broadlands geothermal field, North Island, New Zealand (Torlesse Terrane). This low-permeability fractured greywacke is described as rich in quartz and feldspar minerals, argillite, chlorite stringers, and locally variable quantities of epidote and/or calcite, as well as trace illite, pyrite, muscovite, and secondary potassium feldspar (Hedenquist, 1990; Wood et al, 2001). Petrologic observation, X-ray diffraction, and X-ray fluorescence analysis confirmed this general lithology. Fine-grained clay particles were observed but could not be positively identified.

Inspection of the samples revealed healed and partially healed fractures in the bulk rock, and consequently a larger initial sample was created from the bulk rock such that one healed fracture roughly bisected the sample's long axis. With slight pressure from an arbor press, the sample broke apart along the original fracture. A 30-mm long, 15-mm diameter final cylindrical sample core was produced from the original subsample. The dimensions of the sample were chosen based on the largest possible sample diameter that would allow accurate tomographic characterization as described below. The core halves were re-mated and the ends polished flat. Fluoropolymer material was heat-shrunk over the sample to create a jacket to hold the core halves in place during X-ray tomography scans.

Tomographic data collection

The jacketed fractured core was imaged by X-ray computed microtomography (XRCT) prior to and after reaction at the 8.3.2 beamline at the Advanced Light Source, Lawrence Berkeley National Laboratory. White light (30 keV) was used to collect 2049 angles per tile at a resolution of 4.5 cubic microns/voxel, resulting in 2 sets of approximately 6400 images of core cross-sections perpendicular to the fracture and direction of fluid flow.

Experimental Procedure

Endcaps of C-276 alloy material, outfitted with titanium frits to distribute fluid, were jacketed once and placed at either end of the sample to create a smooth profile. Three additional layers of fluoropolymer heat-shrink material were sealed over the endcaps and sample to create a thick deformable barrier to prevent bypass flow. This sample was then plumbed into the reactor vessel and core-flooding set-up shown in Figure 3.

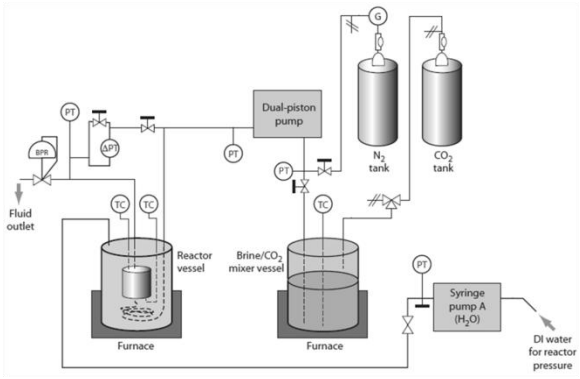

Figure 1: Core-flooding experimental apparatus. BPR, back-pressure regulator; ΔPT/PT, differential/pressure transducer; G, gauge. From Smith et al., 2013.

The sample was brought to a confining pressure of 25 MPa at room temperature by means of a dedicated syringe pump. Saline solutions (0.05m NaCl, CO_2-free) were delivered to the core via a dual-cylinder pulseless pump, while pore pressure/confining pressure ratios were varied to ensure seating of the fracture surfaces. Initial fracture permeability was measured by varying flowrates and observing changes to differential pressure. Sample and fluid temperatures were then ramped to 200 °C overnight, maintaining a constant inlet flowrate of 0.01 mL/min and constant outlet pressure of 8.3 MPa (1200 psi). CO_2-free saline fluid injection continued for approximately two weeks, in order to determine the baseline geochemical response at elevated temperature.

After two weeks of CO_2-free fluid flow, one cylinder of the dual-cylinder pump was purged and reconnected to a pressurized titanium fluid reservoir containing saline solutions equilibrated with and maintained at constant 5.5 MPa pCO_2 pressure. Fluid was continually delivered at a constant flow for the next 49 days, over which time differential pressures across the sample declined to less than 4% of the initial value. After this time, fluid flow was stopped and the sample was brought to atmospheric pressure and temperature as quickly as possible. The innermost fluoropolymer jacket was left intact over the sample to minimize movement of the core halves before post-reaction tomographic imaging.

Geochemical Analysis

Solution chemistry was monitored by collecting fluid samples at the back-pressure regulator output. Prior to the introduction of CO_2, unfiltered samples were collected and analyzed for solution pH at room temperature. After the introduction of CO_2 to the fluid, accurate solution pH measurement was not possible due to CO_2 exsolution at the fluid outlet. Diluted, filtered, and acidified sample aliquots were analyzed for major and trace elements by inductively coupled plasma-mass spectrometry (ICP-MS). Diluted and filtered aliquots were analyzed for chloride, sulfate, and sodium via ion chromatograph (IC) analysis. To monitor total inorganic carbon (TIC), a third aliquot was collected into a glass syringe pre-loaded with 1N NaOH, filtered, and analyzed via a total carbon analyzer.

Mineral saturation indices and *in situ* solution pH reported in following sections were calculated via charge balancing on species H^+ from measured solution compositions and experimental pressure and temperature conditions using the EQ3/6 geochemical speciation code (Wolery, 1992) and the *data.shv* thermodynamic database (Johnson et al., 1992).

Particle Image Velocimetry Analysis

Particle Image Velocimetry (PIV) is a well-established technique used to study fluid motion by tracking bulk movement of carefully selected tracer particles (Adrian, 2005). Here, the same approach is applied to the XRCT data to measure relative displacements in the fractured Ohaaki greywacke sample. Unlike PIV techniques for fluids, the method employed here does not require introduced tracer particles, but rather exploits the latent mineralogical heterogeneity (the grains in XRCT images), thereby non-invasively tracking solid deformation. The XRCT data allows three-dimensional volumes to be compared, unlike the two-dimensional images employed in traditional PIV. The extra information from this added dimension adds to the robustness of the method, allowing accurate displacements to be determined despite measurement artifacts or even chemical alteration (Walsh et al., 2013).

The approach used is similar to that employed in PIV methods for fluids. The pre- and post-reaction tomography datasets are aligned and then segmented into sets of corresponding cubic subregions. The cross correlation between matching subregions is then calculated to obtain a coarse displacement vector from the location of the maximum value. This process is repeated for all subvolumes within the two aligned datasets, giving rise to a displacement field. The original displacement field is then used to improve subvolume comparisons at higher resolution, and the accuracy enhanced further using a sub-pixel interpolation method. These steps are equivalent to the multiresolution approach with discrete window offset employed in traditional PIV methods (e.g., Scarano and Riethmuller, 1999). Once the improved displacement field has been determined, it can be differentiated to find local strains and rotations.

EXPERIMENTAL RESULTS

A representative image of the fracture in cross-section (i.e., perpendicular to the direction of flow) is given in Figure 2. Although several regions of locally wide aperture were identified at points along the fracture, these regions were not interconnected along the long-axis of the sample. The majority of the identifiable fracture aperture was on the order of the XRCT resolution, 1-2 pixels/9 microns wide, complicating its detection by simple image thresholding techniques.

Differential pressure across the core began to decrease as 200 °C fluids passed through the fracture, indicating increasing permeability (see Figure 3). Over 14 days of CO_2-free flow, the differential pressure decreased by over 800 psi, more than 70% of the initial value. With the introduction of CO_2-

enriched fluid, the trend of pressure drop was not immediately affected, although dissolved solute loads increased significantly after this point (see Figure 4).

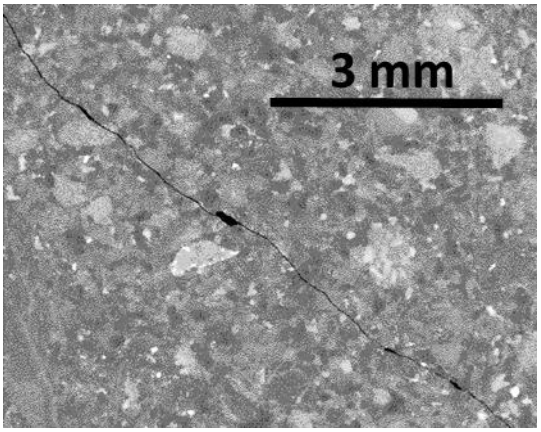

Figure 2: Representative fracture cross-section in x-y plane. XRCT image taken 11 mm from inlet face along long axis of core.

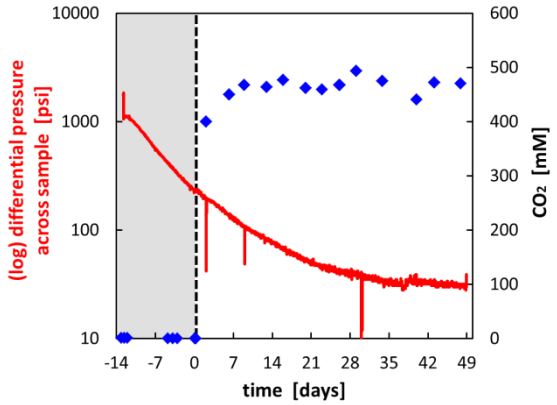

Figure 3: Differential pressure across core (red) and dissolved CO_2 concentration (blue symbols) versus time. Time t=0 indicates the introduction of CO_2 to the system.

During CO_2-free flow periods, dissolved silica levels showed a slight but steadily decreasing trend, while iron levels increased by over an order of magnitude. Other constituents remained at steady levels, at a modeled solution pH of 5.45 (at 200 °C) until the introduction of CO_2 to the system. Immediately following time t = 0, concentrations of calcium, magnesium, and barium (as well as manganese and strontium, not shown) increased significantly, decreasing to pseudo-steady state levels after approximately t = 30 days. Sulfate concentrations showed a delayed peak at t = 7 days and then decreased to pre-CO_2 levels. Silica levels continued to increase over the course of the experiment, in stepped increments. The responses of iron and aluminum were highly variable, and both analytes

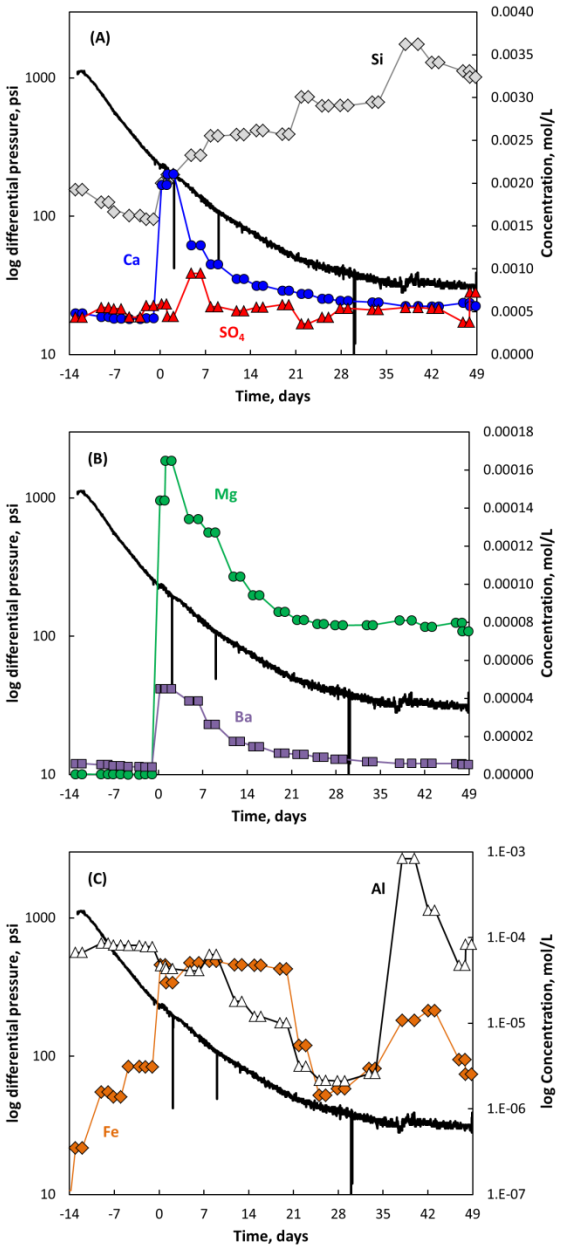

Figure 4: Dissolved concentrations versus time, with (log) differential pressure shown on the left-hand axis. (A) silica, calcium, and sulfate; (B) magnesium and barium; (C) aluminum and iron. Note the log concentration scale in (C). Time t=0 indicates the introduction of CO_2 to the system.

showed marked temporary increases in concentration after a brief (2-minute) pressure drop that occurred at t = 29.9 days. Modeled solution pH remained relatively constant over the period of CO_2-fluid flow, dropping immediately to 4.7-4.5, and then remaining steady after 8 days at a value of 3.90.

Post-reaction tomography imaging revealed that a fully throughgoing dissolution channel developed as the result of sustained 200 °C rock-water±CO_2 interactions. Similar features have been noted previously both experimentally (e.g., Detwiler, 2008) and in numerical studies (Szymczak and Ladd, 2009). A comparison of the final fracture geometry with its initial configuration is shown in Figure 5. This channel developed primarily in the center of the fracture plane, and failed to capture or connect many of the pre-existing wide aperture voidspace regions.

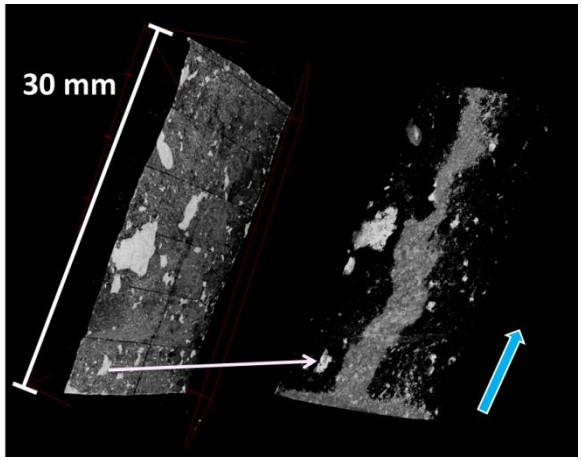

Figure 5: Pre-reaction fracture voidspace (at left) compared to post-reaction fracture voidspace (at right, tilted to provide better view). Wider apertures correspond to brighter white colors. Images are rotated differently; thin white arrow indicates common feature for orientation. Blue arrow indicates direction of fluid flow.

DISCUSSION

Examples of both wallrock dissolution and secondary mineral precipitation were noted within the reacted sample (see Figure 6), although dissolution was the more dominant process by volume. Despite continual dissolution of one or more mineral phases, fracture permeability increased through the development of a dissolution channel centered along the initial fracture plane.

Identification of Reactive Mineral Assemblages

Geochemical modeling of solution chemistry compositions with time provided insight into the potential dissolution and precipitation processes taking place.

Modeled saturation indices, or log (Q/K) values, of representative minerals are shown in Figure 7. We consider first quartz and the feldspars, the most abundant primary mineral phases in the greywacke assemblage. Saturation indices calculated at *in situ* temperature and pressure conditions indicated that solutions remained at or extremely close to equilibrium with quartz over the entire experimental timescale, as silica concentrations approached but remained limited by the solubility of quartz at 200 °C. Solutions became increasingly undersaturated with respect to sodium-bearing feldspars (albite) after CO_2 was introduced to the system. Saturation indices for calcium-bearing feldspars (anorthite) were predicted to be several orders of magnitude lower in these CO_2-enriched fluids. Potassium feldspars, observed as secondary vein-filling precipitates in the altered greywacke (Hedenquist, 1990), remained highly undersaturated in these fluids, as a result of low to non-detectable levels of potassium. Previous modeling work (Wolery and Carroll, 2010) demonstrated that muscovite and potassium feldspar were unstable under similar conditions, and thus the lack of dissolved potassium points to either lower initial quantities or a lack of fluid-accessible reactive surface areas for such potential phase.

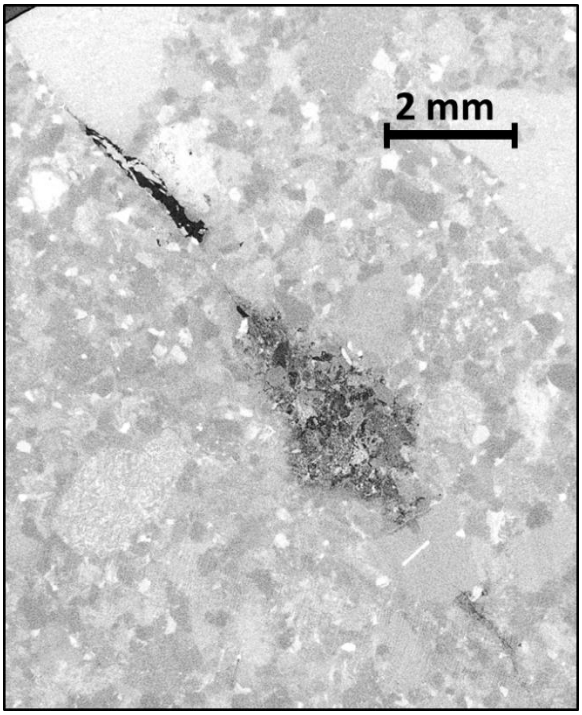

Figure 6: Post-reaction fracture cross-section image at z = 19 mm, showing both precipitated material at upper left and extensive dissolution at center. Note also reduced fracture apertures compared to Figure 2, in regions not experiencing wallrock dissolution.

Preliminary bulk analyses suggested low to trace quantities of calcite in the greywacke samples, but this mineral was expected to be present locally along

portions of the fracture surfaces which were partially healed. Although calcite is highly susceptible to CO_2-driven reaction especially at these low (3.9) *in situ* pH levels, its continual undersaturation in the fluid samples indicated that it may not have been present in large quantities. In contrast, fluids generally remained in equilibrium or slightly supersaturated with respect to barite (another potential secondary alteration or fracture-filling mineral).

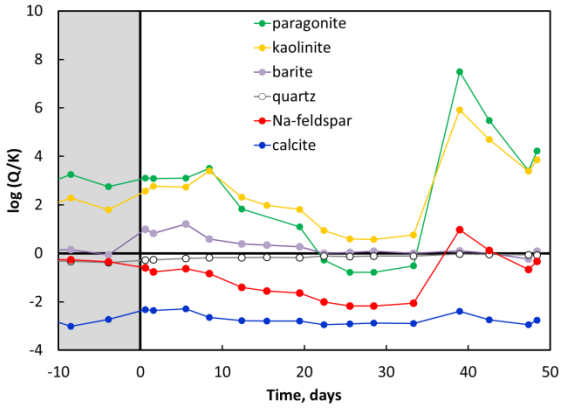

Figure 7: Saturation indices (log Q/K model values) for selected minerals at 200 ℃ versus time. Negative saturation indices indicate potential dissolution while positive values indicate potential for precipitation. Time t=0 indicates the introduction of CO_2 to the system.

Two representative clay and sheet silicate minerals are also shown in Figure 7. Effluent fluids were supersaturated with respect to both kaolinite and paragonite during CO_2-free flow, but after the introduction of $CO_{2(aq)}$, the fluids gradually adjusted towards equilibrium with respect to these minerals (until the depressurization at t = 29.9 days). The steady decrease in aluminum concentrations over the same $0 < t < 29.9$ period may reflect the uptake of aluminum in a clay or sheet silicate-type mineral.

The later-time increase in saturation indices for several phases shown in Figure 7, as well as the increases in many dissolved species in Figure 4, may be related to a short depressurization event in which upstream/inlet pressures decreased below that of the backpressure regulator. This pressure disturbance likely disrupted the established flowpaths within the fracture, and may have forced exchange of fluids between the established dissolution channel and the more isolated regions farther from the channel. Post-reaction tomography showed that in regions far from the dissolution channel, fractures apertures appeared to reduce, effectively creating less mobile zones. In these isolated regions with initially wide aperture, fluids transmitted by high early-time differential pressure gradients may have had longer contact time with wallrock minerals and evolved towards higher levels of dissolved solutes. We see clear evidence of mineral precipitation in these isolated pockets (Figure 6). Disruption of the pressure gradient during the depressurization event may have created a new pathway of exchange between one or more of these isolated regions, thus leading to changes in the overall outlet solution composition.

The geochemical data indicate that a variety of wallrock silicates, including abundant feldspars but also sheet silicates within intergranular space, are highly reactive under these CO_2-enriched conditions. This preliminary analysis also suggests that secondary clays and micas (represented as kaolinite and paragonite in Figure 7) as well as quartz and possibly barite are likely precipitates because these phases are supersaturated or at equilibrium throughout the experiment. The preliminary geochemical model discussed here and concerns on fluid exchange between mobile channel/immobile regions should be tested with more detailed observation of the reaction products and reactive transport simulations capable of incorporating parameter uncertainty (in initial mineral abundance, kinetic dissolution rates, etc.)

Deformation and Porosity Change within the Dissolution Channel

Analysis of fracture segments using the PIV technique adds information to the observations of continuously increasing permeability coupled with ongoing dissolution. The PIV analysis reveals a net movement of the core halves toward each other (as illustrated in Figure 8), as well as fracture aperture reductions in areas that did not experience extensive wallrock dissolution. Overall, no extensive deformation was noted in this sample, but selected particles within regions of focused dissolution could be observed to have rotated and moved from their original position. This "liberation" of less soluble grains has been noted in other experimental work (e.g., Noiriel et al., 2007; Ellis et al., 2011), but it is uncertain what effect such particle movement would have on long-term fracture sustainability.

In addition to quantifying deformation, the PIV technique can also be used to separate its effects from those of chemical alteration. In Figure 9A, pre- and post-reaction cross-sectional XRCT images from a selected location were overlaid, with simple grayscale subtraction used to delineate generated porespace. Such greyscale overlays may generate spurious values in distal regions due to shifts arising from deformation and/or poor image alignment. Using the PIV analysis to correct for the deformation

between the images produces a cleaner result in which most of the spurious values are eliminated (Figure 9B).

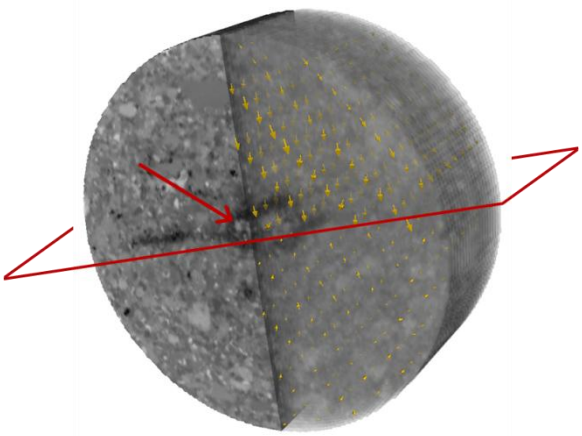

Figure 8: PIV-derived displacement field (displacement vectors in yellow shown in the reference frame of the lower half of the sample). The fracture roughly bisects this view along the plane outlined in red. The small red arrow identifies the fracture dissolution channel developed through intense wallrock dissolution.

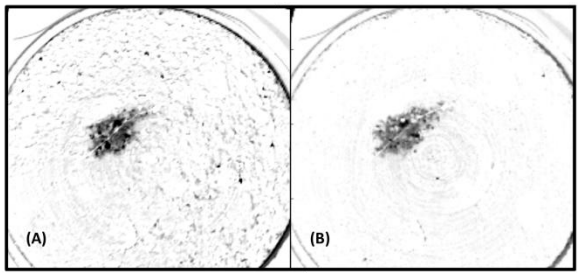

Figure 9: (A) New porespace calculated by image subtraction, versus (B) PIV-corrected porespace refinement. Porespace is shown as darker grayscale colors.

CONCLUSIONS

- During exposure to 200 °C fluids, measured bulk permeability through a natural fracture increased continuously, both before and during CO_2 exposure, indicating that the use of CO_2 and the reaction of CO_2-enriched fluids with reservoir materials was beneficial to fracture and permeability sustainability.
- As a result of focused dissolution, a central throughgoing fracture channel developed, extending into the wallrock (perpendicular to the fracture plane).
- Tomographic imaging demonstrated that focused dissolution was the dominant process, but also revealed examples of mineral precipitation in isolated, off-channel regions of initially wide aperture.
- Particle image velocimetry (PIV) results indicate a net movement of core halves toward each other, with fracture aperture reduction greatest in competent areas not experiencing wallrock dissolution.
- In regions of inter-grain dissolution within the developed channel, PIV analysis identified three-dimensional rotation of solid particles or grains liberated by dissolution. It is uncertain whether transport of such particles in a larger fracture system would sustain permeability (by emplacing particles as natural proppants) or degrade fracture permeability (by clogging downstream fluid pathways).

ACKNOWLEDGMENTS

This work was supported by the United States Department of Energy's Geothermal Technologies Program. We would like to acknowledge Rick Kemptner, Jeff Roberts, and Dave Ruddle (LLNL) for technical support; Dula Parkinson (LBNL) for tomography expertise; and Andrew Rae and Ed Mroczek (GNS Science) for the greywacke rock samples and Ohaaki fluid chemistry data.

DISCLAIMER

REFERENCES

Adrian, R. J. (2005). "Twenty years of particle image velocimetry". Experiments in Fluids, 39(2), 159-169.

Brown, D.W. (2000), "A hot dry rock geothermal energy concept utilizing supercritical CO_2 instead of water," Proc., 25th Workshop on Geothermal Reservoir Engineering, Jan. 24-26, Stanford University, Stanford, CA pp233-238.

Carlson, S.R., Roberts, J.J., Detwiler, R.L., Vianai, B.E., and Roberts, S.K. (2005), "Fracture permeability evolution in Desert Peak quartz monzonite," *Geothermal Resources Council Transactions*, **29**, 337-342.

Detwiler, R.L. (2008), "Experimental observations of deformation caused by mineral dissolution in variable-aperture fractures," *Journal of Geophysical Research*, **113**, B08202.

Ellis, B., Peters, C., Fitts, J., Bromhal, G., McIntyre, D., Warzinski, R., and Rosenbaum, E. (2011), "Deterioration of a fractured carbonate caprock exposed to CO_2-acidified brine flow," *Greenhouse Gases Science and Technology*, **1**, 248-260.

Hedenquist, J.W. (1990), "The thermal and geochemical structure of the Broadlands-Ohaaki geothermal system, New Zealand," *Geothermics*, **19**, 151-185.

Johnson, J.W., Oelkers, E.H., and Helgeson, H.C. (1992), "SUPCRT92: A software package for calculating the standard molal thermodynamic properties of minerals, gases, aqueous species, and reaction from 1 to 5000 bar and 0 to 1000 °C," *Computational Geosciences*, **98**, 131-139.

McGrail, B.P., Schaef, H.T., Glezakou V.A., Dang, L.X., and Owen, A.T. (2009), "Water reactivity in the liquid and supercritical CO_2 phase: Has half the story been neglected?," *Energy Procedia*, **1**, 3415-3419.

Morrow, C.A., Moore, D.E., and Lockner, D.A. (2001), "Permeability reduction in granite under hydrothermal conditions," *Journal of Geophysical Research*, **B12**, 30551-30560..

Noiriel, C., Madé, B., and Gouze, P. (2007), "Impact of coating development of the hydraulic and transport properties in argillaceous limestone fracture," *Water Resources Research*, **43**, W09406.

Polak, A., Elsworth, D., Yasuhara, Y., Grader, A.S., and Halleck, P.M. (2003), "Permeability reduction of a natural fracture under net dissolution by hydrothermal fluids," *Geophysical Research Letters*, **30**, 2020.

Polak, A., Elsworth, E., Liu, J., and Grader, A.S. (2004) "Spontaneous switching of permeability changes in a limestone fracture with net dissolution," *Water Resources Research*, **40**, W03502.

Pruess, K. (2006), "Enhanced geothermal systems (EGS) using CO_2 as working fluid – A novel approach for generating renewable energy with simultaneous sequestration of carbon," *Geothermics*, **35**, 351-367.

Scarano, F., and Riethmuller, M.L. (1999), "Iterative multigrid approach in PIV image processing with discrete window offset," *Experiments in Fluids*, 26, 513-523.

Smith, M.M., Wolery, T.J., and Carroll, S.A. (2013), "Kinetics of chlorite dissolution at elevated temperatures and CO_2 conditions," *Chemical Geology*, in revision.

Smith, M.M., Sholokhova, Y., Hao, Y., and Carroll, S.A. (2013), "Evaporite caprock integrity: An experimental study of reactive mineralogy and pore-scale heterogeneity during brine-CO_2 exposure," *Environmental Science & Technology*, **2**, 262-268.

Suto, Y., Liu, L., Yamasaki, N., and Hasida, T. (2007), "Initial behavior of granite in response to injection of CO_2-saturated fluid," *Applied Geochemistry*, **22**, 202-218.

Szymczak, P., and Ladd, A.J.C. (2009), "Wormhole formation in dissolving fractures," *Journal of Geophysical Research*, **114**, B06203.

Ueda, A., Kato, K., Ohsumi, T., Yajima, T., Ito, H., Kaieda, H., Metcalfe, R., and Takase, H. (2005), "Experimental studies of CO_2-rock interaction at elevated temperatures under hydrothermal conditions," *Geochemical Journal*, **39**, 417-425.

Walsh, S.D.C., DuFrane, W.L., Mason, H.E., and Carroll, S.A. (2013), "Permeability of wellbore-cement fractures following degradation by carbonated brine," *Rock Mechanics and Rock Engineering*, in press.

Wolery, T.W. (1992), "EQ3/6, a software package for geochemical modeling of aqueous systems," UCRL-MA-110662-PT-1, Lawrence Livermore National Laboratory, Livermore, CA.

Wolery, T.W., and Carroll, S.A. (2010), "CO_2-rock interactions in EGS-CO_2: New Zealand TVZ geothermal systems as a natural analog," *Geothermal Resources Council Transactions*, **34**, 670-677.

Wood, C.P., Brathwaite, R.L., and Rosenberg, M.D. (2001), "Basement structure, lithology and permeability at Kawerau and Ohaaki geothermal fields, New Zealand," *Geothermics*, **30**, 461-481.